Fibers and Polymers 2019, Vol.20, No.2, 375-383
DOI 10.1007/s12221-019-8910-3

ISSN 1229-9197 (print version)
ISSN 1875-0052 (electronic version)

Simulation of Multi-cavity Micro-injection System for Reducing Cavity Filling Deviation

Beom Rae Kim[1], Sung Nam Moon[2], Sung Ho Park[3], Woo Il Lee[1], and Seung Mo Kim[4]*

[1]*Department of Mechanical Engineering, College of Engineering, Seoul National University, Seoul 08826, Korea*
[2]*LG Chemical, Daejeon 34122, Korea*
[3]*Samsung Display, Yongin 17113, Korea*
[4]*Department of Mechanical Engineering, Korea University of Technology and Education, Cheonan 31253, Korea*

(Received September 29, 2018; Revised November 7, 2018; Accepted November 9, 2018)

Abstract: In micro-injection molding, it is important to make each cavity filled uniformly. However, there are several factors that cause deviation in cavity filling. These factors include the mold temperature differential between runners and the diameter differential of gates or runners caused by mold manufacturing tolerances. In this study, we conducted numerical analysis to identify the major factors that cause cavity filling deviation and suggest a considerably robust design for micro-injection mold to minimize the deviation. In the numerical simulation, we used thermophysical property values of EP-7000, one of the polycarbonate series polymers used for injection molding. The Cross-Arrhenius model was adopted with regard to the viscosity of the polymer. To model the specific heat and the thermal conductivity, we used the piecewise-linear method. Further, the volume of fluid method and the piecewise-linear interface scheme were used to visualize the polymer flow. Sixteen-cavity injection mold was modeled, and simulations were done for four different variations (the mold temperature, the runner diameter, the gate thickness, and a combination of the mold temperature and the runner diameter). Numerical analysis indicated that the case of mold temperature exhibited a difference of up to 28 % in instant cavity filling rate and the case of combination showed a difference of up to 33 %. We suggested designs employing convergent runner and resin reservoir to reduce deviation. As a result, the convergent runner design could reduce the instant cavity filling rate deviation by 20 %, while the resin reservoir design reduced the deviation by 18 %. The combination of these two could reduce the deviation by up to 22 %.

Keywords: Injection molding, Flowmark, Simulation, Robust design, CFD

Introduction

Micro-injection molding (MIM) is one of the key process for manufacturing thermoplastic microproducts or microparts and is widely used as a cost effective replication method for mass production [1]. For a good replication of microparts, there are certain major process parameters: mold temperature, injection speed, injection pressure, holding time, holding pressure, etc. [2-5]. These parameters are directly related to the factors that determine the quality of microproducts. Especially, surface quality is an important factor for micro-optical products such as microlens.

MIM comprises largely of the following three steps: (a) the mold cavity equipped with a microstructured tool (mold insert) is closed, evacuated, and heated above the glass transition temperature of the polymer. (b) an injection unit heats the polymer and presses the viscous polymer into the mold. (c) the polymer (and the tool) is cooled below its glass transition temperature and demolded from the tool [6]. Several surface defects may be obtained while the resin is being filled in the second step. Several of those defects are complimented by the high pressure in the packing stage after the second step, but some defects like weld lines, sink marks, and flow marks remain after the packing stage [7].

Recent studies are focused on establishing the cause of the surface defects or decreasing them by changing the parameters in experiments and visualizing unstable flow front using CFD simulations. However, in multi-cavity system, the balance regarding the filling of each cavity is also important. Different studies investigate the relation between the parameters and cavity filling [8,9], or the effect of mold geometry on cavity filling [10,11], but there are not many studies focused on cavity filling deviation of multi-cavity systems.

Thus, our study is focused on observing the major process condition that causes flux non-uniformity in multi-cavity micro-injection molding system and suggesting the flow network for complementing the cavity filling deviation. We refer to this flow network as robust design. We constructed 16-cavity micro-injection mold and investigated the relation between the cavity filling deviation and three parameters: wall temperature, runner diameter, and gate size. Moreover, based on these results, we propose three robust designs: convergent model, reservoir model, and complex model (combination of the convergent and reservoir models), and observed the effect of these models on reducing the cavity filling deviation.

Theory

Governing Equations

The motion of polymer resin is governed by the

*Corresponding author: smkim@koreatech.ac.kr

conservation of mass and momentum. These conservation equations can be written for laminar flow as

$$\frac{\partial \rho}{\partial t}+\frac{\partial(\rho u)}{\partial x}+\frac{\partial(\rho v)}{\partial y}+\frac{\partial(\rho w)}{\partial z}=S_m \tag{1}$$

$$\frac{\partial}{\partial t}(\rho\bar{v})+\nabla\cdot(\rho\bar{v}\bar{v})=-\nabla p+\nabla\cdot(\bar{\bar{\tau}})+\rho\bar{g}+\bar{F} \tag{2}$$

Equation (1) is the general form of the mass conservation equation and is valid for incompressible as well as compressible flow. ρ is the density, u, v, and w are the velocity components in the x, y, and z directions, respectively, and S_m is the mass added to the continuous phase from the dispersed second phase (for example, due to vaporization of liquid droplets). In this study, we did not consider phase changes, thus, we assumed that S_m=0. And the material is assumed to be incompressible during the filling stage for convenience. This assumption means that the density of the polymer resin is constant, so the first term of the equation (1) is neglected.

Equation (2) is the momentum conservation equation where p is the static pressure, $\bar{\tau}$ is the stress tensor, and $\rho\bar{g}$ and $\bar{F}$ are the gravitational body force and external body forces (for example, the ones that arise occur from interaction with the dispersed phase), respectively. As the phase change and the gravity force are neglected, $\bar{F}$=0 . The stress tensor $\bar{\tau}$ is given by

$$\bar{\tau}=\mu\left[\left(\nabla\bar{v}+\nabla\bar{v}^T-\frac{2}{3}\nabla\cdot\bar{v}I\right)\right] \tag{3}$$

where μ is the viscosity, I is the unit tensor, and the second term on the right hand side is the effect of volume dilation.

To include heat transfer in our simulation, an additional equation for energy conservation is solved.

$$\frac{\partial}{\partial t}(\rho E)+\nabla\cdot(\bar{v}(\rho E+\rho))=\nabla\cdot\left(k_{eff}\nabla T-\sum_j h_j\vec{J}_j+(\bar{\bar{\tau}}_{eff}\cdot\vec{v})\right) \tag{4}$$

where K_{eff} is the effective thermal conductivity and $\vec{J}_j$ is the diffusion flux of species j. The first three terms on the right-hand side represent the energy transfer due to conduction, species diffusion, and viscous dissipation, respectively. And E and h are given by,

$$E=h-\frac{p}{\rho}+\frac{v^2}{2} \tag{5}$$

$$h=\sum_j Y_j h_j+\frac{p}{\rho} \tag{6}$$

In equation (5), Y_j is the mass fraction of species j and

$$h_j=\int_{T_{ref}}^{T} C_{p,j}dT \tag{7}$$

The value used for T_{ref} is 298.15 K.

Models for Thermophysical Propertites of Polymer

The widely accepted Cross-Arrhenius model is adopted with regard to the viscosity of the polymer material. The non-Newtonian behavior of the molten polymer can be characterized using this model. The Cross-Arrhenius model has temperature and shear rate as dependent factors, and the model is given by

$$\eta=H(T)\frac{\eta_0}{1+(\lambda\dot{\gamma})^{1-n}} \tag{8}$$

$$H(T)=\exp\left[\alpha\left(\frac{1}{T-T_0}-\frac{1}{T_\alpha-T_0}\right)\right] \tag{9}$$

where η_0 is zero-shear-rate viscosity, λ is time, $\dot{\gamma}$ is share rate, and n is power-law index. λ is the inverse of the shear rate where the fluid viscosity changes from Newtonian to power-law behavior. $H(T)$ is the temperature dependence, known as Arrhenius law. α is the ratio of the activation energy to the thermodynamic constant and T_α is a reference temperature for which $H(T)$=1. T_0 is the temperature shift, and we set it to 0.

For characterizing the specific heat (C_P) and thermal conductivity (k), we used the piecewise-linear method. The piecewise-linear method is described for finding and optimal segment approximation to specified functions from discrete data by a number of connected straight-line segments [12,13]. For example of specific heat, we set 12 points of specific heat as a function of temperature obtained from the experimental procedures and assumed the values between each point in the neighborhood to be linear. The thermal conductivity is characterized by the same method. We assumed that the properties of air and mold are constants.

Numerical Conditions

Values for Material Models

For the numerical analysis, we used the thermal characteristic values of the polymer resin in the polycarbonate series. As mentioned above, the polymer material is assumed to be incompressible. So, the density of the polymer material is constant in the entire simulation process, and its value is given as, ρ=1250 kg/m^3. The Cross-Arrhenius model constants for the viscosity of the polymer material are shown in Table 1. Also, the piecewise-linear values of specific heat and

Table 1. Cross-Arrhenius model constants for polymer material

Symbol	Quantity
Zero shear viscosity, η_0 (kg/m·s)	5280
Power law index, n	0.269
Time constant, λ (s)	0.009216
Reference temperature, T_α (K)	530.1209
Activation energy/R, α(K)	17373.33

Table 2. Piecewise-linear values of specific heats for polymer material

Temperature (K)	304.15	341.15	363.15	376.15	384.15	392.15
C_P (J/kg·K)	1130	1310	1408	1470	1512	1570
Temperature (K)	400.15	405.15	410.15	420.15	477.15	533.15
C_P (J/kg·K)	1690	1794	1874	1913	2015	2082

Table 3. Piecewise-linear values of thermal conductivity for polymer material

Temperature (K)	310.65	325.25	345.25	365.35	385.55	405.65
k (w/m·K)	0.146	0.146	0.146	0.15	0.153	0.164
Temperature (K)	425.15	444.35	463.65	483.45	503.15	522.85
k (w/m·K)	0.192	0.192	0.192	0.192	0.193	0.197

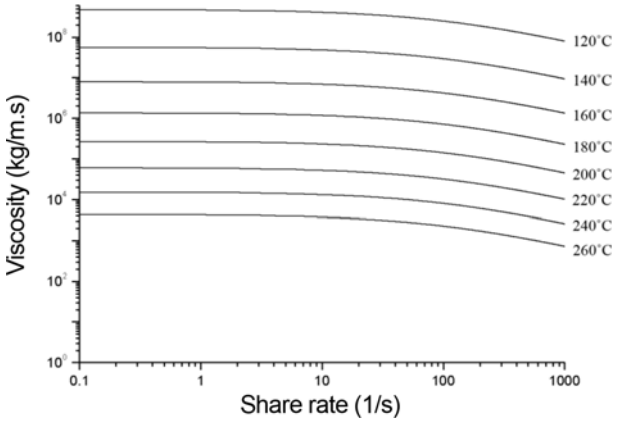

Figure 1. Cross-Arrhenius model for polymer material.

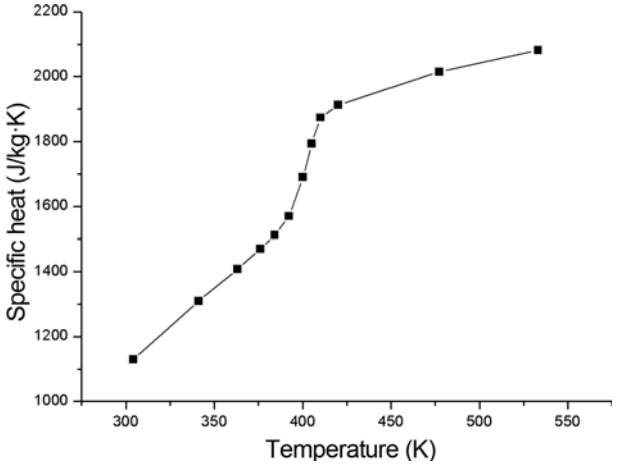

Figure 2. Specific heat for polymer material.

thermal conductivity for the polymer material are listed in Tables 2 and 3, respectively.

Figure 1 shows the Cross-Arrhenius model with respect to values in Table 1. It indicates the viscosity of the polymer material used in this study based on the temperature and shear rate, and the temperature range in the entire simulation

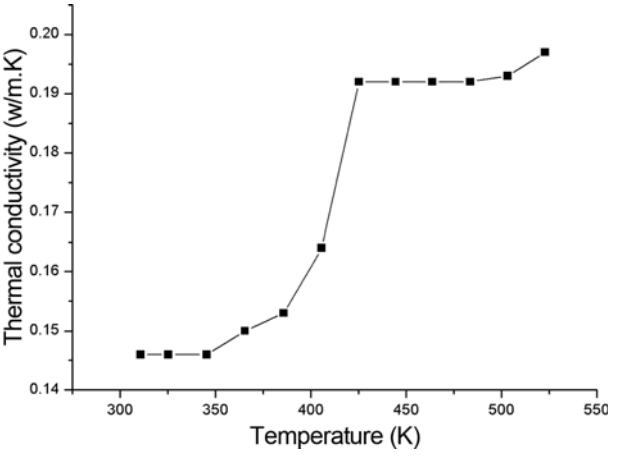

Figure 3. Thermal conductivity for polymer material.

process is 130 °C to 260 °C. As the injection time is short and the injection temperature of the polymer resin is 260 °C, the substantive temperature range is approximately 200 °C to 260 °C except at the near-wall region. Figures 2 and 3 show the specific heat and the thermal conductivity of the polymer material based on temperature, respectively.

As mentioned before, the property values of the mold material and air are assumed to be constants for convenience of calculation. The density, specific heat, and thermal conductivity of the mold material are 8030 kg/m^3, 502.48 J/kg·K, and 16.27 W/m·K, respectively. Air is considered as an ideal gas, and the density, the specific heat, the thermal conductivity, and the viscosity of air are 1.225 kg/m^3, 1006.43 J/kg·K, 0.0242 W/m·K, and 1.7894×10^{-5} kg/m·s, respectively.

Mold Geometry and Meshing

To observe the primary cause of cavity filling deviation, we considered a multi-cavity micro injection mold. Figure 4(a) shows the model that we used for our simulation. As can be seen, there is one sprue, intersection of first runners, 8 first runners, and 16 second runners. For each component, different meshing skills were used. The resin is injected into

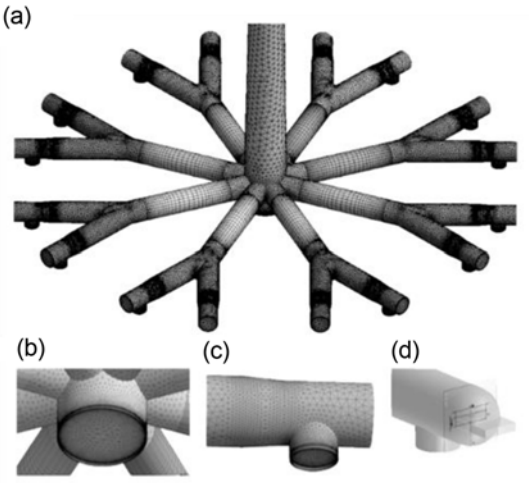

Figure 4. (a) Model and meshing for simulation, (b) intersection of first runners, (c) end of second runner, and (d) shape of gates.

the top of the sprue, and it flows through the first and second runners, subsequently, it comes out to the gate outlet. We assumed that the mass of each cavity is 5.6 mg, so if the accumulated resin outlet mass flow of each outlet reaches 5.6 mg, we assumed the cavity is completely filled. The number of elements is approximately 2.5 million. It can be observed that in Figures 4(b) and (c), there are air vents at the end of the intersection and the second runners, and the thickness of those vents is 50 μm. Moreover, we placed the gates at each end of the second runners and the shape of these gates is shown in Figure 4(d). The gates are rectangular in shape and the width is 1.26 mm.

Boundary Conditions

Figure 5 shows the boundary conditions used in the simulations. In actual process for manufacturing multi-system micro injection mold, it is hard to make all runners and gates in exactly same size. And these errors can affect the flow of resin polymer which causes cavity filling deviation. In addition, keeping all runners at the same temperature is not an easy process so there can be small differences in the temperature of each runner. These small differences in temperature can have a significant effect on the behavior of polymer, so it can be the major factor for the cavity filling deviation. Therefore, we used the following three primary factors that cause cavity filling deviation: mold temperature, runner diameter, and gate size. The complex case illustrated in Figure 5(d) is the combination of the mold temperature case and the runner diameter case. The boundary conditions of this complex case are described in Table 4 and the reason for using this combination without the gate size case will be explained in the result section. We

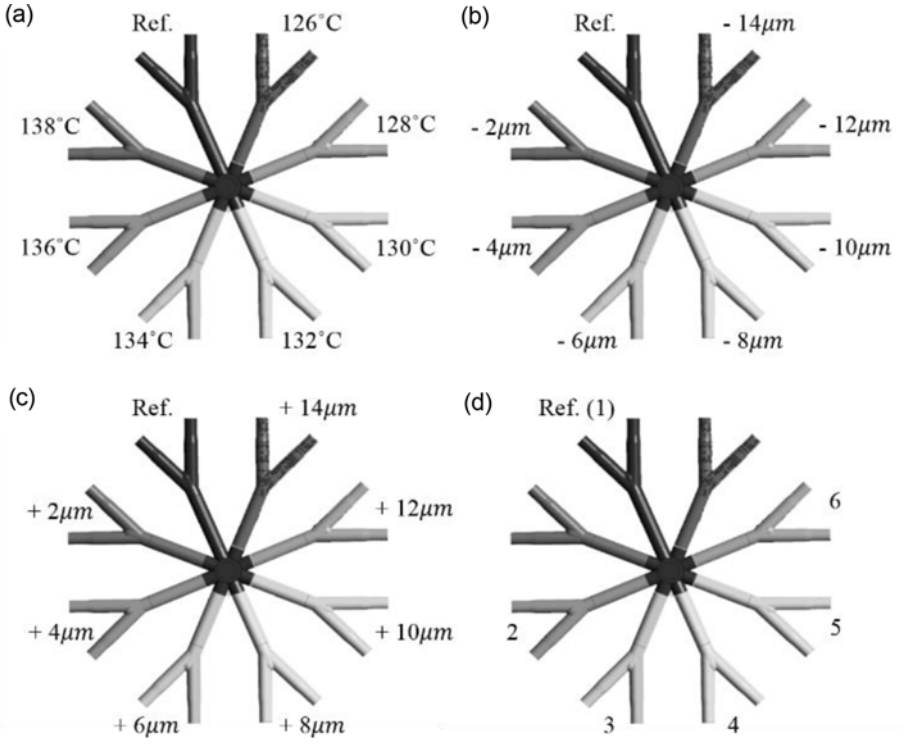

Figure 5. Boundary conditions for our simulation (a) mold temperature case (reference temperature is 140 °C), (b) runner diameter case (reference diameter is 2.3 mm), (c) gate thickness case (reference thickness is 0.3 mm), and (d) complex case (reference mold temperature is 140 °C and reference runner diameter is 2.3 mm).

Table 4. Boundary conditions for complex case

No.	1	2	3
Conditions	Original condition (140 °C, 2.3 mm)	Wall temperature -4 °C Runner diameter -4 μm	Wall temperature -6 °C Runner diameter -6 μm
No.	4	5	6
Conditions	Wall temperature -8 °C Runner diameter -8 μm	Wall temperature -10 °C Runner diameter -10 μm	Wall temperature -12 °C Runner diameter -12 μm

set the reference boundary conditions same as general process conditions for manufacturing micro lens and give variety to other conditions. The range of runner diameter and gate size are same as the errors in actual process, but we exaggerated the runner temperature boundary conditions for simulation convenience in comparison with the actual process. In actual process, the range of runner temperature is in less than 2 K.

Results and Discussion

Cavity Filling Deviation

First, in Figure 6, the outlet mass flow rate of the resin is presented. The yellow box in this figure refers to the time when each cavity is completely filled. Therefore, the start line of the yellow box is the time when the first cavity is completely filled, and the end line of that box is the time when the last cavity is completely filled. The width of the yellow box refers to the difference in time when the first and the last cavity is completely filled, and we call it "filling time delay." Further, the time deviation when each flow reaches the gate outlet can be observed; the time deviation of the mold temperature case and the runner diameter case are similar, but the gate size case exhibits the smallest time deviation.

When the first cavity is completely filled, we named the filling rate of other cavities at that time as "filling fraction," and it is presented in Figure 7. The square dots in this figure represent the delay time: cavity filling time differences between the first cavity and each subsequent cavity. So, the

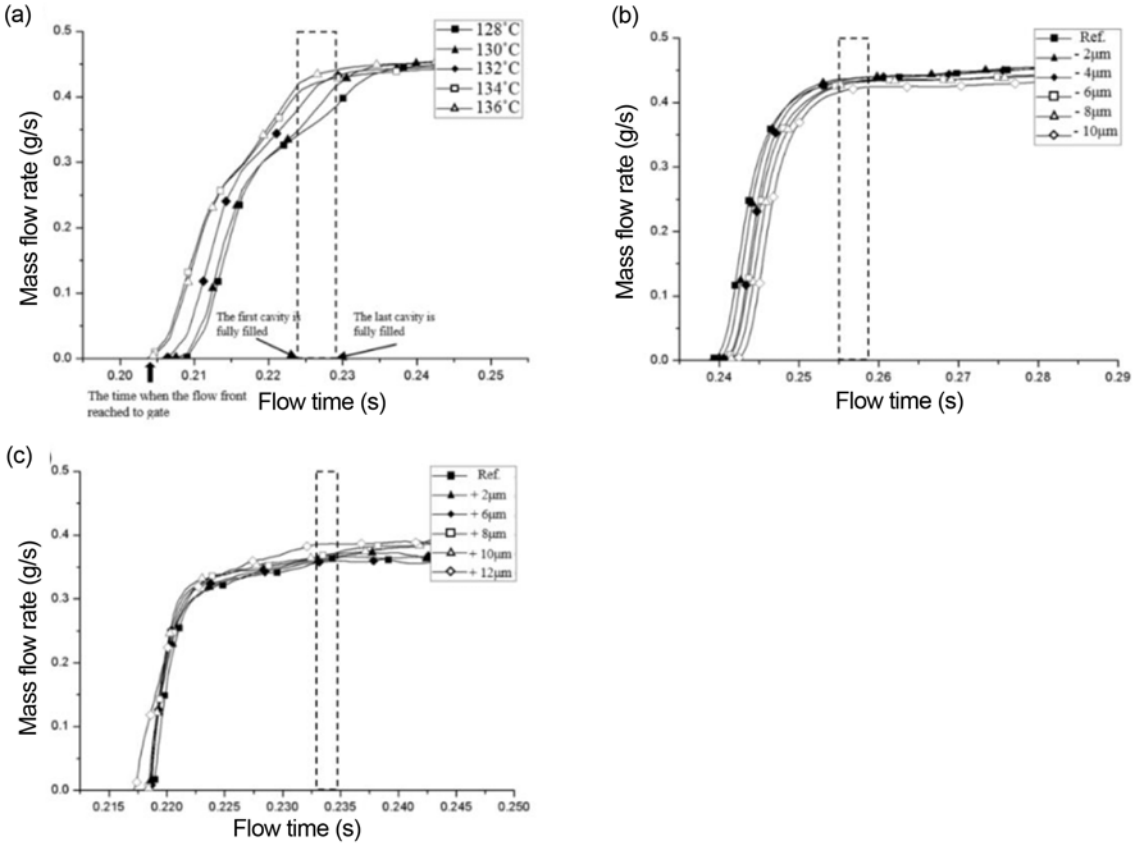

Figure 6. Resin outlet mass flow rate in gate of each runner (a) mold temperature case, (b) runner diameter case, and (c) gate size case.

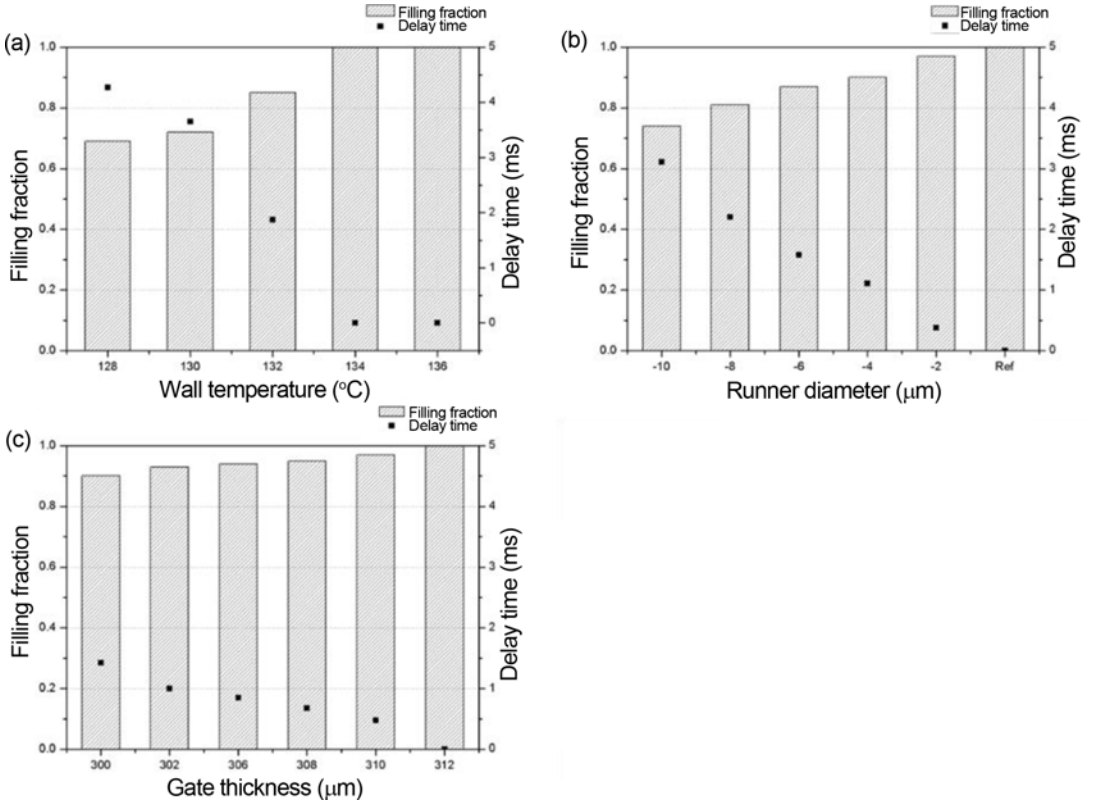

Figure 7. Delay time and filling fraction of each cavity (a) wall temperature case, (b) runner diameter case, and (c) gate size case.

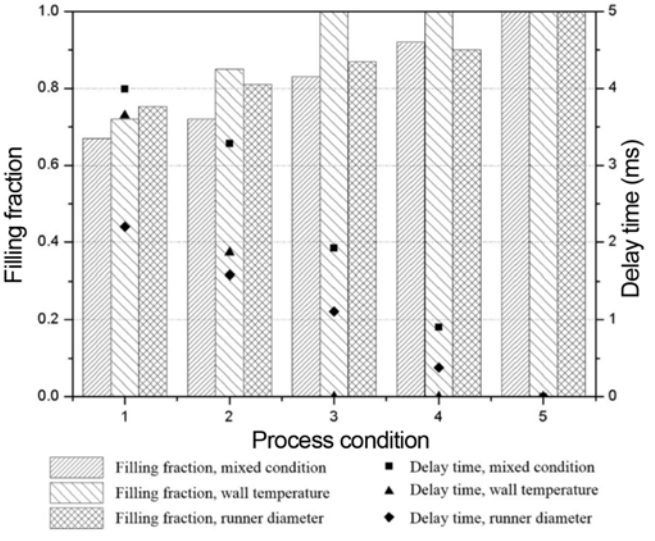

Figure 8. Delay time and filling fraction of each case.

biggest delay time is the same as the filling time delay. Similar to the result in Figure 6, the gate size exhibits the smallest differences in both filling fraction and delay time deviation. Thus, we decided that the primary causes of cavity filling deviation are the differences of wall temperature and runner diameter, so we combined those two cases in the complex case.

The results of three cases - mold temperature variation, runner diameter variation, and complex case are described in Figure 8. The specific boundary conditions for Figure 8 is shown in Table 5. It is noted that considering the actual process condition, the difference in wall temperature between each runner is a bit exaggerated. As expected, the complex case has the worst filling uniformity. This case had the smallest filling fractions and delay times on every boundary condition in comparison to other cases. The numerical values regarding the filling time delay and the highest filling fraction difference are shown in Table 6. The

Table 5. Boundary conditions for results in Figure 8

No.	1	2	3	4	5
Wall temperature case	-10 °C	-8 °C	-6 °C	-4 °C	Ref
Runner diameter case	-10 μm	-8 μm	-6 μm	-4 μm	Ref
Complex case	Wall temperature -10 °C Runner diameter -10 μm	Wall temperature -8 °C Runner diameter -8 μm	Wall temperature -6 °C Runner diameter -6 μm	Wall temperature -4 °C Runner diameter -4 μm	Ref

Table 6. Filling time delay and biggest filling fraction difference of each case

Simulated cases	Wall temperature	Runner diameter	Gate size	Complex condition
Filling time delay	3.65 ms	3.11 ms	1.43 ms	3.99 ms
Biggest filling fraction difference	28 %	26 %	10 %	33 %

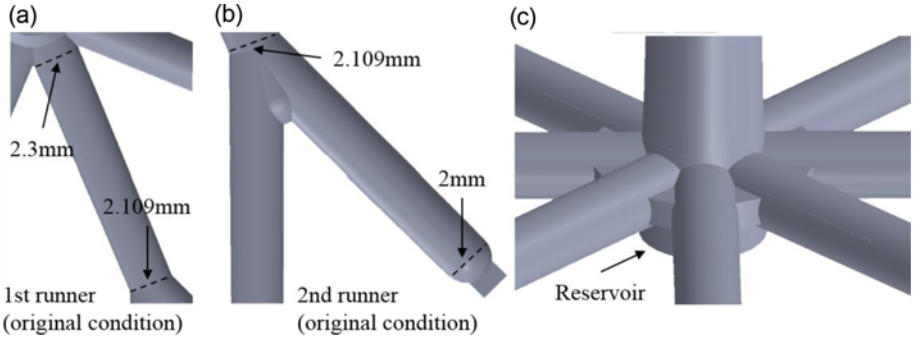

Figure 9. Geometry of robust designs (a) and (b) convergent runner model, and (c) reservoir model.

filling fraction difference was 33 % and filling time delay was 3.99 ms in the complex case.

Robust Design for Reducing Cavity Filling Deviation

To reduce cavity filling deviation we simulated and suggested three new models - convergent runner model, reservoir model, and complex model, which is the combination of the other two models. The geometry of these models is described in Figure 9. Figure 9(a) and (b) shows the convergent runner model, (c) is the reservoir model, and the complex model is a combination of both. Using the three models, we calculated their effects on reducing cavity filling deviation. For comparison, we used boundary conditions of the complex case that we simulated.

In order to demonstrate the effectiveness of the robust model, we considered the head loss of a convergent channel. Head loss is defined as the energy loss by friction between the fluid and wall. The head loss in a channel with variable cross-sectional area is given by […]

$$\Delta h = \int_L \pi d \tau_w dl = \int_L \frac{32 \mu Q}{d^2} dl \tag{10}$$

where h is the head loss, τ_w is the shear stress at the wall surface, l is the length of the runner, μ is the viscosity of fluid, Q is the flux, and d is the diameter of the runner. For a convergent channel, the head loss grows non-linearly with the distance. This is in contrast to the case of a channel with constant cross-section as illustrated in Figure 10.

As the flow front in the runner goes downstream, due to the increased head loss, the speed of flow front slows down. Therefore, even if there exists a difference in the flow front location among runners in the beginning, this difference tends to become smaller as the flow front advances in the convergent runner.

Thus, we set the diameter of every end of the second runners as 2 mm and changed the diameter of the entrance of each first runners same as the complex case in the previous simulation, which subsequently rendered all runners convergent. The boundary conditions regarding wall temperature are same as the complex case. For the reservoir model, we introduced the reservoir on the first runner intersection of our system. The diameter of this reservoir was 7.8 mm and the thickness was 0.5 mm. The boundary conditions of the reservoir model were same as the complex case.

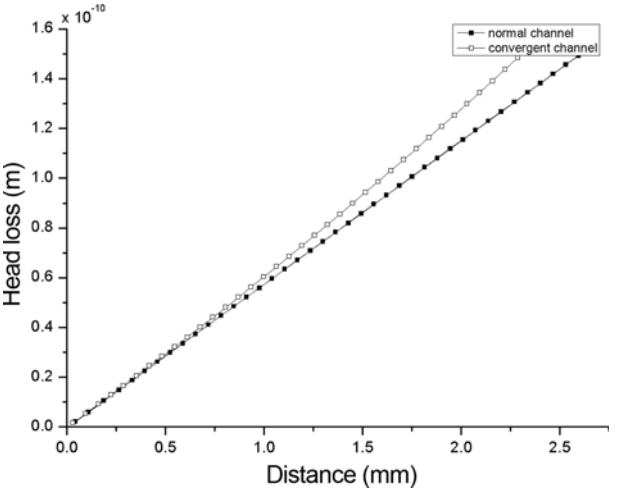

Figure 10. Head loss increase comparison between normal channel and convergent channel.

The effects of the proposed robust designs are summarized in Figures 11 and 12. In the convergent model, there exists a new interval (0.225-0.232 ms) when the deviation between the outlet mass flow of each gate decreases. After that time, the deviation increases again, but when we consider the mass of the cavity (5.6 mg), all cavities are fully filled before

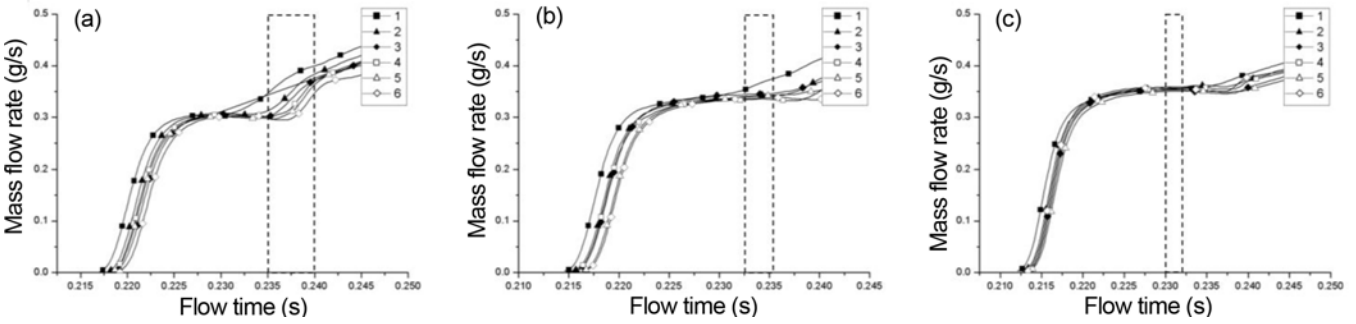

Figure 11. Outlet mass flow of each model (a) convergent model, (b) reservoir model, and (c) complex model.

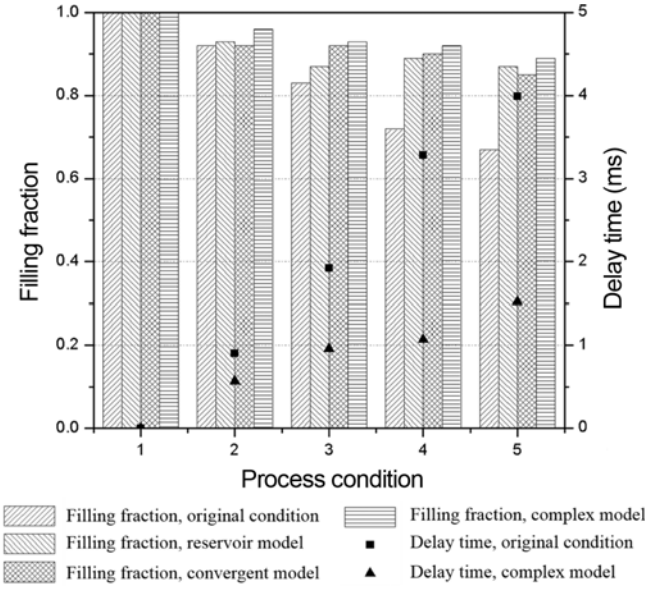

Figure 12. Filling fraction and delay time of robust designs.

the difference of flux increases more than the normal channel model. Subsequently, the cavity filling deviation in convergent channel is reduced in comparison to normal channel.

Moreover, the arrival time of the flow front to the gate and the difference between each runner decreased. Compared with the result of the original complex case, the deviation of the arrival time and cavity filling time decreased by 62 % and 48 %, respectively. Also, the largest filling fraction deviation decreased by 20 %. In the reservoir model, there is similar interval (where the deviation between outlet mass flow of each gate decreases) with regards to the convergent model in 0.224-0.232 ms. After that time, the deviation between the outlet mass flow was more stable than the convergent model. The deviation of the arrival time and the cavity filling time decreased by 48 % and 46 %, respectively, and the highest filling fraction difference decreased by 18 % in comparison to the original complex boundary condition. It is because the resin flow pooled into the reservoir until it reached a certain amount. Subsequently, the flows with similar amount proceeded from the reservoir through each runner. Further, the reservoir shortened the runner length which had non-uniformity, and it made the resin flow stable. For the complex model, the most stable outlet mass flow was observed, the arrival time was the fastest, and the deviation between each runner was the smallest. The deviation of the arrival time, cavity filling time, and the highest filling fraction difference decreased by 60 %, 62 %, and 22 %, respectively, and this was the best result obtained from our models.

Conclusion

We studied the cavity filling deviation in micro-injection molding with 16 cavity models by using numerical analysis. Considering the actual process condition, the effect of the wall temperature on the cavity filling deviation was not important. On the other hand, considering the actual process condition function, the difference in runner diameter of approximately 10 μm the highest filling fraction difference was 26 %. Based on these results, we noted that the cavity filling deviation is considerably dependent on the runner diameter. The effect of the gate size was also insignificant. For the worst, we combined the wall temperature case and the runner diameter case into the complex case. In this case, the filling fraction difference was 33 % and the filling time delay was 3.99 ms and the cavity filling deviation was indeed higher than the other cases.

To reduce the cavity filling deviation, we suggested three robust models: convergent channel model, reservoir model, and complex model. Because of the equilibrating effect regarding the flow front in the convergent channel, the cavity filling deviation decreased in the convergent model. Moreover, the reservoir model had certain effect on reducing the cavity filling deviation. The combination of the two models exhibited the best result in reducing cavity filling deviation; the deviation of the arrival time, cavity filling time, and the highest filling fraction difference decreased by 60 %, 62 %, and 22 %, respectively.

The mold temperature difference and the runner diameter

difference can be the major cause of cavity filling deviation in multi-cavity micro-injection system. To reduce such deviation, we proposed three robust designs, and observed the effects of those designs. The convergent runners and the reservoir in multi-cavity mold can be a satisfactory solution for reducing cavity filling deviation in multi-cavity micro-injection systems. The combination of those two designs led to even better improvement.

Acknowledgments

This work was supported by Civil-Military Technology Cooperation Program funded by the Ministry of Trade, Industry & Energy. (No. 13-DU-MP-17-MKE) and Basic Science Research Program through the National Research Foundation of Korea (NRF) funded by the Ministry of Education (NRF-2017R1D1A1B03035636).

References

1. C. A. Griffiths, S. S. Dimov, E. B. Brousseau, and R. T. Hoyle, *J. Mater. Process Technol*., **189**, 418 (2005).
2. J. Giboz, T. Copponnex, and P. Mélé, *J. Micromech. Microeng*, **17**, R96 (2007).
3. B. R. Whiteside, M. T. Martyn, and P. D. Coates, *Int. Polym. Process*, **20**, 162 (2005).
4. J. Zhao, R. H. Mayes, G. Chen, H. Xie, and P. S. Chan, *Polym. Eng. Sci*., **43**, 1542 (2003).
5. J. Zhao, R. H. Mayes, G. Chen, P. S. Chan, and Z. J. Xiong, *Plast. Rubber Compos*., **32**, 240 (2003).
6. M. Heckele and W. K. Schomburg, *J. Micromech. Microeng*., **14**, R1 (2004).
7. M. F. Lacrampe and J. Pabiot, *J. Inject. Molding Technol*., **4**, 167 (2000).
8. L. Yu, C. G. Koh, L. J. Lee, and K. W. Koelling, *Polym. Eng. Sci*., **42**, 871 (2002).
9. Y. Su, J. Shah, and L. Lin, *J. Micromech. Microeng*, **14**, 415 (2004).
10. C. Wu and W. Liang, *Polym. Eng. Sci*., **45**, 1021 (2005).
11. H. L. Zhang, N. S. Ong, and Y. C. Lam, *Int. J. Adv. Manuf. Technol*., **37**, 1105 (2008).
12. A. Cantoni, *IEEE Trans. Comput*., **C-20**, 59 (1971).
13. B. Hamann and J.-L. Chen, *Comput. Aided Geometric Des.,* **11**, 289 (1994).
14. S. H. Park, S. M. Kim, S. Y. Kang, W. I. Lee, and Y. E. Yoo, *Int. Polym. Process*, **27**, 205 (2012).